Hindawi
Complexity
Volume 2018, Article ID 4140762, 15 pages
https://doi.org/10.1155/2018/4140762

WILEY | Hindawi

Research Article

Chaos and Symbol Complexity in a Conformable Fractional-Order Memcapacitor System

Shaobo He,[1,2] Santo Banerjee,[3,4] and Bo Yan[2]

[1]*School of Physics and Electronics, Central South University, Changsha 410083, China*
[2]*School of Computer Science and Technology, Hunan University of Arts and Science, Changde 415000, China*
[3]*Institute for Mathematical Research, Universiti Putra Malaysia, Serdang, Selangor, Malaysia*
[4]*Malaysia-Italy Centre of Excellence for Mathematical Science, Universiti Putra Malaysia, Serdang, Selangor, Malaysia*

Correspondence should be addressed to Santo Banerjee; santoban@gmail.com

Received 27 April 2018; Accepted 5 July 2018; Published 5 August 2018

Academic Editor: Viet-Thanh Pham

Application of conformable fractional calculus in nonlinear dynamics is a new topic, and it has received increasing interests in recent years. In this paper, numerical solution of a conformable fractional nonlinear system is obtained based on the conformable differential transform method. Dynamics of a conformable fractional memcapacitor (CFM) system is analyzed by means of bifurcation diagram and Lyapunov characteristic exponents (LCEs). Rich dynamics is found, and coexisting attractors and transient state are observed. Symbol complexity of the CFM system is estimated by employing the symbolic entropy (SybEn) algorithm, symbolic spectral entropy (SybSEn) algorithm, and symbolic C_0 ($SybC_0$) algorithm. It shows that pseudorandom sequences generated by the system have high complexity and pass the rigorous NIST test. Results demonstrate that the conformable memcapacitor nonlinear system can also be a good model for real applications.

1. Introduction

In 1971, Chua postulated the concept of memristor that describes a relationship between flux and charge [1]. In 2008, researchers in Hewlett-Packard announced that a solid-state implementation of memristor has been successfully fabricated [2]. Since then, designing memory circuits has received significant attention of researchers, and many different kinds of memristor-based circuits have been designed [3–5]. In 2009, Ventra et al. [6] reported memcapacitors and meminductors. Compared with memristors, memcapacitors and meminductors have received much less attention. Currently, memcapacitor and meminductor can be designed based on the memristor. For example, Biolek and Biolkova [7] designed a memcapacitor model based on memristor by means of off-the-shelf circuits. As a matter of fact, memory electronic elements are usually designed nonlinearly. Thus, chaos can be easily found in those memory electronic element-based circuits [8–16]. Bao et al. [8–11] presented many valuable works on chaotic memristor circuits. For instance, their most recent work reported quasiperiodic behavior and chaotic busting in a third-order autonomous memristive oscillator [11]. Moreover, Mou et al. [12] designed a memory circuit with two memcapacitors that exhibited complex phenomena of state transition and transient chaos accompanied with time evolution and coexisting states. Fractional calculus has been studied for about 300 years, and there are a large number of literatures reporting chaos in the fractional-order nonlinear systems [17–20]. Moreover, fractional-order memory electronic element-based systems increasingly attracted attention of scholars [21, 22]. Since not much research exists about the fractional-order memcapacitor system, a fractional-order system with two memcapacitors is considered in this paper.

All of the abovementioned systems are integer-order systems or fractional-order chaotic systems under Caputo

definition or Riemann-Liouville (R-L) definition [23]. In 2014, Khalil et al. [24] proposed a new fractional derivative, and it is called the conformable fractional (CF) derivative. Since the CF definition is prominently compatible with the integer-order derivative, it has been widely studied in different research fields [25–28]. For example, İskender Eroğlu et al. [26] proposed an optimal boundary temperature control for a time-conformable fractional heat conduction equation. However, to our best knowledge, there are only two literatures reporting numerical analysis of CF chaotic systems. He et al. [29] firstly solved the nonlinear CF equations by the conformable Adomian decomposition method (CADM) and found chaos in the CF simplified Lorenz system. Later, Ruan et al. [30] investigated dynamics of a CF memristor system based on CADM, and rich dynamical behaviors were found. It shows that the CF nonlinear systems also generate chaos, and it is an interesting topic to explore complexity in these systems. Recently, Ünal and Gökdoğan [31] modified the differential transform method (DTM) and applied this method to solve CF nonlinear equations. But it has not been used to solve CF chaotic systems. Thus, in this paper, we will use conformable DTM to solve the CF memcapacitor system and analyze this system numerically.

Meanwhile, measuring complexity is also an important method to analyze dynamics of chaotic systems. It reflects the security of the system to some extent. When a system has higher complexity, it means that the time series generated by the system is more random. Currently, there are several methods to measure complexity of time series, such as the permutation entropy (PE) [32], sample entropy (SampEn) [33], spectral entropy (SE) [34], and C_0 algorithms [35]. It should be noted out that complexity of chaotic systems is mainly estimated based on the original time series, and complexity analysis of nonlinear symbol sequence has aroused interests of researchers [36, 37]. Meanwhile, there are many kinds of pseudorandom sequence generation algorithms. How complexity and dynamics of a chaotic system are determined by the pseudorandom quantization algorithms should be investigated. And whether the CFM system can be actually used in real applications should be verified.

The rest of the article is organized as follows. In Section 2, definitions of conformable fractional derivative and a numerical solution algorithm are proposed. Solution of the CFM system is obtained. In Section 3, dynamics of the CFM system is analyzed by means of Lyapunov characteristic exponents (LCEs), bifurcation diagram, and phase portraits. In Section 4, three different symbol complexity measuring algorithms are designed and the complexity of the CFM system is analyzed. Meanwhile, the NIST test is carried out. Finally, we summarize the results in Section 5.

2. Definitions and Numerical Solution Algorithm

In this section, the system model and definitions about conformable fractional derivative are presented. A numerical solution algorithm for conformable fractional nonlinear systems is designed based on the differential transform method.

Table 1: Parameters for the three kinds of chaotic attractors.

Type	(a_1, b_1)	(a_2, b_2)
I	(−0.17, 10)	(0.25, 0.6)
II	(0.15, 10)	(−0.2, 0.6)
III	(−0.17, 10)	(−0.2, 0.6)

2.1. The Conformable Fractional Memcapacitor System. Mou et al. [12] proposed a circuit with memcapacitor, and it is denoted by

$$\begin{aligned} \dot{x} &= cf_1(z), \\ \dot{y} &= (d-e)f_2(y) + ef_1(z), \\ \dot{z} &= e(f_2(y) - f_1(z)) - x, \end{aligned} \tag{1}$$

where c, d, and e are the system parameters, x, y, and z are the state variables, and $f_1(z) = a_1 z + b_1 z^3$ and $f_2(y) = a_2 y + b_2 y^3$ represent the two memcapacitors in the circuit in which a_1, b_1, a_2, and b_2 are the intrinsic parameters of the two memcapacitors. In [12], $c = 8.96$, $d = 4$, and e is the bifurcation parameter. Moreover, there are three different sets of intrinsic parameters for different types of attractors. The three sets of intrinsic parameters are shown in Table 1.

By introducing the conformable fractional derivative to the system, the conformable fractional memcapacitor (CFM) system is defined as

$$\begin{aligned} T_{t_0}^{q_1} x &= cf_1(z), \\ T_{t_0}^{q_2} y &= (d-e)f_2(y) + ef_1(z), \\ T_{t_0}^{q_3} z &= e(f_2(y) - f_1(z)) - x, \end{aligned} \tag{2}$$

where $T_{t_0}^{q}$ is the conformable fractional derivative and $0 < q_1, q_2, q_3 \leq 1$. Definitions and characteristics of the conformable fractional derivative are given as follows.

Definition 1 [24]. For a given function $f : [0, \infty) \to R$, its conformable fractional derivative of order α is defined by

$$T_{t_0}^{q} f(t) = \lim_{\varepsilon \to 0} \frac{f\left(t + \varepsilon t^{1-q}\right) - f(t)}{\varepsilon}, \tag{3}$$

where $t > t_0 \geq 0$ and $q \in (0, 1]$.
Let $q \in (0, 1]$ and f, g be q-differentiable at a point $t > t_0 \geq 0$. Then,

(1) $T_{t_0}^{q}(af + bg) = a(T_{t_0}^{q} f) + b(T_{t_0}^{q} g)$, for all $a, b \in \mathbb{R}$;

(2) $T_{t_0}^{q}(t^p) = pt^{p-q}$, for all $p \in \mathbb{R}$;

(3) $T_{t_0}^{q}(\lambda) = 0$, for all constant functions $f(t) = \lambda$;

(4) $T_{t_0}^{q}(fg) = f(T_{t_0}^{q} g) + g(T_{t_0}^{q} f)$;

(5) $T_{t_0}^{q}(f/g) = (g(T_{t_0}^{q} f) - f(T_{t_0}^{q} g))/g^2$;

(6) $T_{t_0}^{q} f(t) = t^{1-q}(df/dt)(t)$.

Definition 2 [24]. The conformable fractional integral of function $f : [q, \infty) \to \mathbb{R}$ is defined by

$$\left(I_{t_0}^{q} f\right)(t) = \int_{t_0}^{t} \frac{f(x)}{(x - t_0)^{1-q}} dx, \tag{4}$$

where $t > t_0 \geq 0$, $q \in (0, 1]$, and f is q-differentiable at $[t_0, t]$.

2.2. Conformable Fractional Differential Transform Method. The differential transform method is one of the most effective methods for semianalytic analysis of differential equations. Here, the conformable fractional differential transform method (CFDTM) is introduced to solve the conformable fractional chaotic system.

Assume that f is an infinitely q-differentiable function, for $0 < q \leq 1$ at a neighborhood of a point t_0. Then, f has the fractional power series expansion [31].

$$f(t) = \sum_{k=0}^{\infty} \frac{\left(T_{t_0}^{q} f\right)(t_0)(t - t_0)^{qk}}{q^k k!}, \tag{5}$$

where $t_0 < t < t_0 + R^{1/q}$, $R > 0$, and $\left(T_{t_0}^{q} f\right)^{(k)}(t_0)$ denotes the conformable fractional derivative for k times. Define the conformable fractional differential transform of $f(t)$ as

$$F_q(k) = \frac{1}{q^k k!} \left[\left(T_{t_0}^{q} f\right)^{(k)}(t)\right]_{t=t_0}, \tag{6}$$

where $\left(T_{t_0}^{q} f\right)^{(k)}(t)$ denotes the application of the fractional derivative for k times. Thus, the inverse conformable fractional differential transform of $F(k)$ is defined as

$$f(t) = \sum_{k=0}^{\infty} F_q(k)(t - t_0)^{qk}. \tag{7}$$

Lemma 1 [31]. *If $f(t) = u(t) \pm v(t)$, then $F_q(k) = U_q(k) \pm V_q(k)$.*

Lemma 2 [31]. *If $f(t) = \alpha u(t)$, then $F_q(k) = \alpha U_q(k)$.*

Lemma 3 [31]. *If $f(t) = u(t)^3 = u(t)u(t)u(t)$, then $F_q(k) = \sum_{i=0}^{k}\sum_{j=0}^{i}\sum_{l=0}^{j} U_q(l)U_q(j-l)U_q(k-j)$.*

The multistep CFDTM method is proposed to solve the CFM system. Divide the time interval $[0, T]$ into small subintervals $[t_n, t_{n+1}]$, where $n = 0, 1, 2, \ldots, N$, $t_N = T$, and $t_{n+1} - t_n = h$. According to (7), the solution of the system over interval $[t_n, t_{n+1}]$ is given by

$$\begin{aligned} x(t_{n+1}) &\approx \sum_{k=0}^{D} X(k) h^{kq_1}, \\ y(t_{n+1}) &\approx \sum_{k=0}^{D} Y(k) h^{kq_2}, \\ z(t_{n+1}) &\approx \sum_{k=0}^{D} Z(k) h^{kq_3}, \end{aligned} \tag{8}$$

where

$$\begin{aligned} X(k+1) &= \frac{1}{q_1(k+1)} cF_1^k, \\ Y(k+1) &= \frac{1}{q_2(k+1)} \left[(d-e)F_2^k + eF_1^k\right], \\ Z(k+1) &= \frac{1}{q_3(k+1)} \left[e\left(F_2^k - F_1^k\right) - X(k)\right], \end{aligned} \tag{9}$$

and

$$\begin{aligned} F_1^k &= a_1 Z(k) + b_1 \sum_{i=0}^{k}\sum_{j=0}^{i}\sum_{l=0}^{j} Z(l)Z(j-l)Z(k-j), \\ F_2^k &= a_2 Y(k) + b_2 \sum_{i=0}^{k}\sum_{j=0}^{i}\sum_{l=0}^{j} Y(l)Y(j-l)Y(k-j). \end{aligned} \tag{10}$$

It should be pointed out that

$$\begin{aligned} X(0) &= x(t_n), \\ Y(0) &= y(t_n), \\ Z(0) &= z(t_n). \end{aligned} \tag{11}$$

It means that $x(t_{n+1})$, $y(t_{n+1})$, and $z(t_{n+1})$ can be obtained based on $x(t_n)$, $y(t_n)$, and $z(t_n)$, and the solution can be given as $\mathbf{x}(t_{n+1}) = F(\mathbf{x}(t_n))$. As for the contribution of this section, there are two aspects that could be specified. Firstly, it is the first time that the solution of the conformable fractional-order chaotic (memcapacitor) system is obtained by employing DTM. Secondly, we modified the method as the multistep CFDTM method by dividing the solution into subintervals $[t_n, t_{n+1}]$, and the obtained solution can be represented as $\mathbf{x}(t_{n+1}) = F(\mathbf{x}(t_n))$. Thus, the numerical solution of the conformable fractional-order chaotic system can be obtained in MATLAB.

In addition, we choose $D = 3$ for the approximation of the system. Let $e = 6.9$; phase diagrams with different derivative orders are shown in Figure 1. As shown in Figure 1, type I and type III attractors do not change much with the decrease of derivative orders while type II attractor is changed from chaos to periodical circle. Obviously, these three types of attractors are different. According to [12], there is no steady state in the type I system and type III system, but the type II system is steady when $0 < e < 4$.

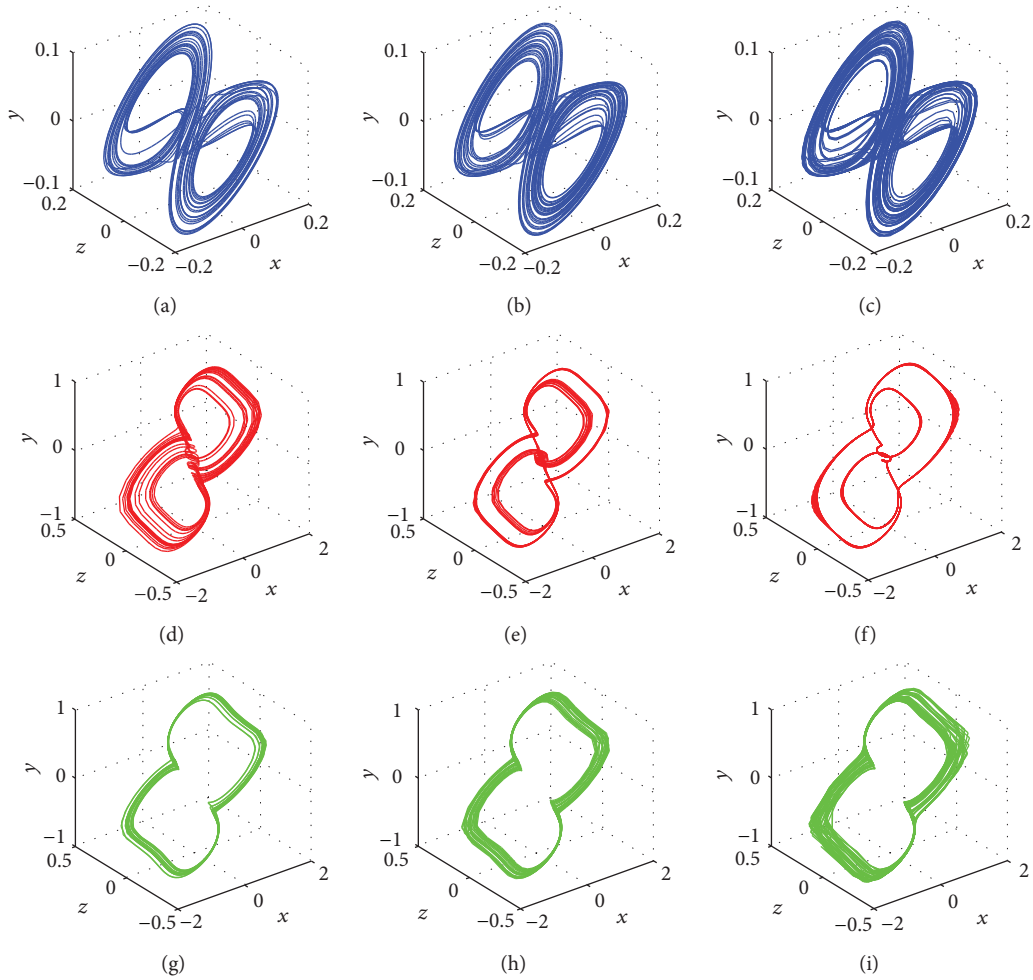

Figure 1: Different types of chaotic attractors in the CFM system with different fractional derivative orders: (a) type I attractor with $q_1 = q_2 = q_3 = 0.95$; (b) type I attractor with $q_1 = q_2 = q_3 = 0.9$; (c) type I attractor with $q_1 = q_2 = q_3 = 0.8$; (d) type II attractor with $q_1 = q_2 = q_3 = 0.95$; (e) type II attractor with $q_1 = q_2 = q_3 = 0.9$; (f) type II attractor with $q_1 = q_2 = q_3 = 0.8$; (g) type III attractor with $q_1 = q_2 = q_3 = 0.95$; (h) type III attractor with $q_1 = q_2 = q_3 = 0.9$; (i) type III attractor with $q_1 = q_2 = q_3 = 0.8$.

3. Dynamical Analysis of the CFM System

3.1. LCE Calculation Algorithm. As mentioned above, the solution of the CFM system can be written as $\mathbf{x}(t_{n+1}) = F(\mathbf{x}(t_n))$; thus, it is actually shown as a given map $\mathbf{x}(n+1) = F(\mathbf{x}(n))$. Here, the QR decomposition method is employed to calculate the LCEs of the system. The computational process is denoted as

$$qr[\mathbf{J}_n\mathbf{J}_{n-1}\cdots\mathbf{J}_1] = qr[\mathbf{J}_n\mathbf{J}_{n-1}\cdots\mathbf{J}_2(\mathbf{J}_1\mathbf{Q}_0)] = \mathbf{Q}_n\mathbf{R}_n\cdots\mathbf{R}_2\mathbf{R}_1, \tag{12}$$

where $qr[\cdot]$ represents the QR decomposition function, $\mathbf{J}$ is the Jacobian matrix of the given map, $\mathbf{Q}$ is an orthogonal matrix, and $\mathbf{R}$ is an upper triangular matrix. All LCEs are calculated according to the upper triangular matrix, and they are given by [38]

$$\lambda_\eta = \frac{1}{Mh}\sum_{i=1}^{M}\ln|R_i(\eta,\eta)|, \tag{13}$$

where $\eta = 1, 2, 3$ (dimension of the system) and M is the maximum iteration number. Here, the Jacobian matrix is obtained by the MATLAB symbolic operation function $J =$ Jacobian$(\cdot)$. LCEs of attractors in Figure 1 are calculated, and the results are shown in Table 2.

Table 2: LCEs of the CFM system with different derivative orders.

Type	$q_1 = q_2 = q_3 = 0.95$	$q_1 = q_2 = q_3 = 0.90$	$q_1 = q_2 = q_3 = 0.80$
I	0.0987, 0, −3.4849	0.1290, 0, −4.7279	0.2287, 0, −8.4289
II	0.1099, 0, −6.422	0.0855, 0, −7.1556	0, 0, −16.1767
III	0.0531, 0, −9.0147	0.0789, 0, −12.4373	0.2831, 0, −28.5537

3.2. Bifurcation and Chaos. As with [12], we also treat parameter e as a bifurcation parameter. Meanwhile, dynamics with the variation of fractional derivative orders q_1, q_2, and q_3 is also analyzed. Since type II attractor changes more with the decrease of derivative orders, it is chosen as the representation of the three kinds of chaotic attractors for further

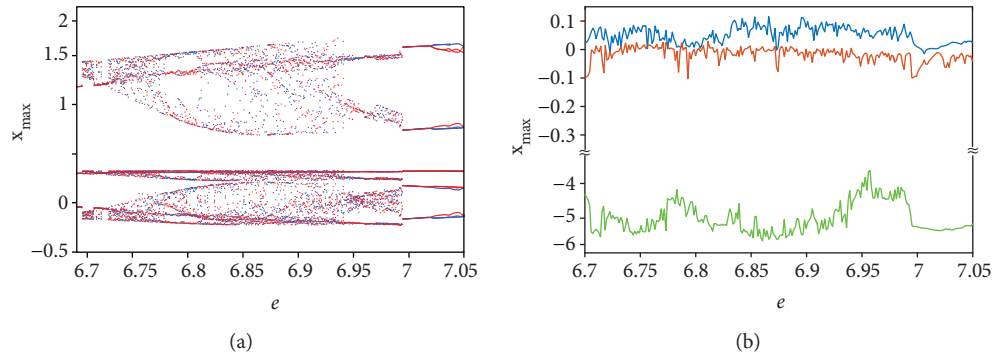

Figure 2: Dynamics of the CFM system with parameter e varying: (a) bifurcation diagram; (b) LCEs.

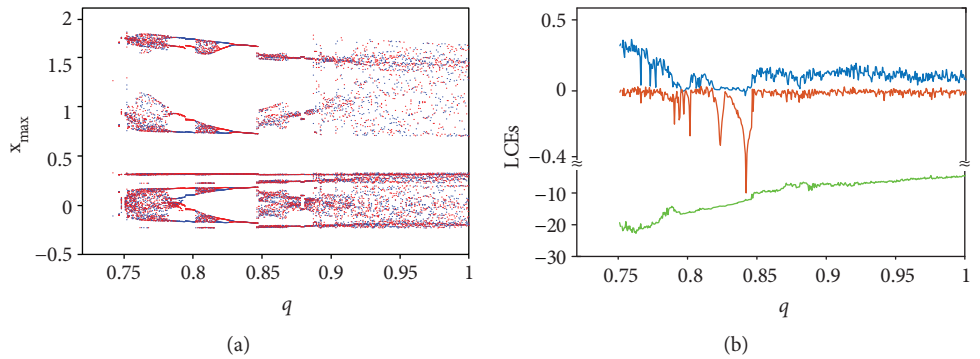

Figure 3: Dynamics of the CFM system with derivative order $q_1 = q_2 = q_3 = q$ varying: (a) bifurcation diagram; (b) LCEs.

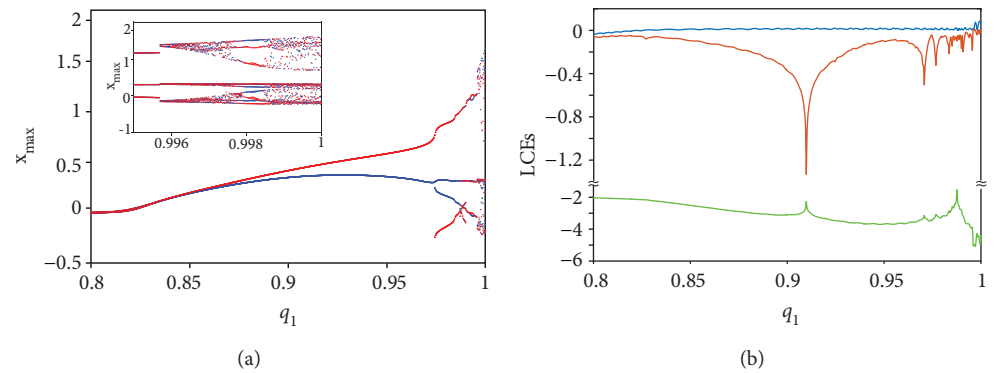

Figure 4: Dynamics of the CFM system with derivative order $q_2 = q_3 = 1$ and q_1 varying: (a) bifurcation diagram; (b) LCEs.

analysis. When plotting bifurcation diagrams, the initial condition for the blue dots is $[x(t_0), y(t_0), z(t_0)] = [0.1, 0, 0]$, while the initial condition for the red dots is $[x(t_0), y(t_0), z(t_0)] = [-0.1, 0, 0]$.

Case 1. Fix $q_1 = q_2 = q_3 = 0.95$ and vary parameter e from 6.7 to 7.05 with a step size of 0.0007. The bifurcation diagram and LCEs with parameter e varying are shown in Figure 2. It shows that dynamical behaviors of the CFM system change with the variation of parameter e. The system is chaotic when $q \in [6.7, 0.7561]U[0.7617, 6.9974]$, while the system is periodical when $q \in (0.7561, 0.7617)U(6.9974, 7.05)$.

Case 2. Let $e = 6.9$ and $q_1 = q_2 = q_3 = q$. Vary q from 0.72 to 1 where the variation step size is 0.002. As shown in Figure 3(a), the system is divergent when $q < 0.75$. When $q \in [0.7568, 0.802]U(0.817, 0.8496)$, the system is periodical while the chaotic interval is $q \in [0.75, 0.7568]U(0.802, 0.817)U[0.8496, 1]$. LCE curves agree well with the analysis results. It shows that rich dynamics is found with the decrease of q.

Case 3. Let $e = 6.9$ and $q_2 = q_3 = 1$, and vary q_1 from 0.995 to 1 with a step size of 0.00056. The bifurcation diagram and its corresponding LCEs are shown in Figure 4. The system is

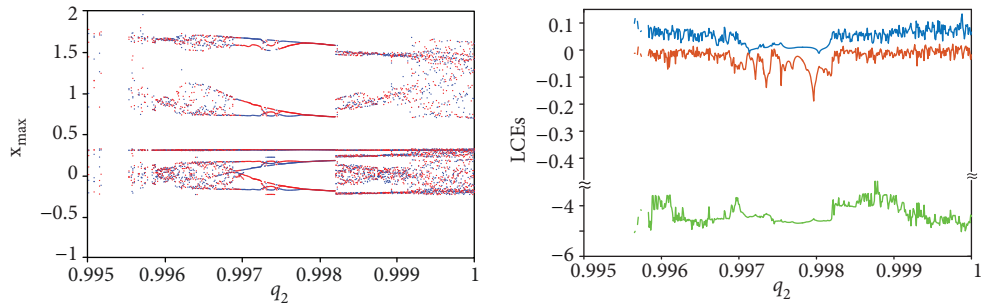

(a) (b)

Figure 5: Dynamics of the CFM system with derivative order $q_1 = q_3 = 1$ and q_2 varying: (a) bifurcation diagram; (b) LCEs.

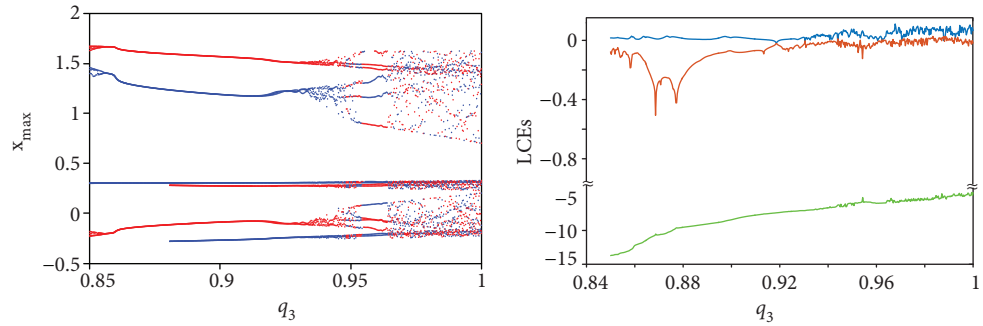

(a) (b)

Figure 6: Dynamics of the CFM system with derivative order $q_2 = q_2 = 1$ and q_3 varying: (a) bifurcation diagram; (b) LCEs.

chaotic when $q \in [0.9958, 0.9975]U[0.9984, 1]$, while the system is nonchaotic for the rest values of q_1.

Case 4. Let $e = 6.9$ and $q_1 = q_3 = 1$, and vary q_2 from 0.995 to 1 with a step size of 0.00001. The bifurcation diagram and its corresponding LCEs are shown in Figure 5. When $q_2 < 0.9959$, the transient state is found. The system is chaotic at the beginning and then becomes divergent finally. The system is periodical when $q \in [0.9967, 0.9982]$, while for the rest range, the system is chaotic.

Case 5. Let $e = 6.9$ and $q_1 = q_2 = 1$, and vary q_3 from 0.995 to 1 with a step size of 0.00001. The bifurcation diagram and its corresponding LCEs with derivative order q_3 are shown in Figure 6. The system is chaotic when $q \in [0.942, 0.95]U[0.961, 1]$, and the system is periodical when $q \in [0.85, 0.942]U[0.95, 0.961]$.

As shown above, after introducing the conformable fractional derivative, the system still has rich dynamical behaviors like parameter e and derivative orders q_1, q_2, and q_3. Moreover, when varying one derivative order and the other two to be equal to 1, the chaotic region shrinks much, compared with that when all derivative orders are varied simultaneously. The minimum order for chaos in the CFM system is 2.25, when the system is solved by CFDTM. Meanwhile, according to Figures 3–6, the system is chaotic when $q_1 = q_2 = q_3 = 1$. However, when the derivative orders become smaller, the periodical state can be observed. It means that derivative orders can change the dynamics of the system distinctly. Thus, the conformable derivative orders q_1, q_2, and q_3 are also the bifurcation parameters. Chaotic pseudorandom sequence (CPRS) has been widely used in real applications. In the next section, complexity of the CPRS generated by the CFM system is measured and the potential application values of the system are discussed.

3.3. Coexisting Attractors and Transient State. As shown in the above bifurcation diagrams, when the initial conditions are different, the red and blue dots show two different routes to chaos. Moreover, the coexistence of multiple attractors is produced mainly due to the reason that symmetry and invariance exist in the system. For the CFM system, it is symmetric and invariant under the transformation $(x, y, z) \to (-x, -y, -z)$ for all values of parameter e. Thus, the coexistence of multiple attractors should be observed. As mentioned above, two different sets of initial conditions are chosen which are $[x(t_0), y(t_0), z(t_0)] = [0.1, 0, 0]$ and $[x(t_0), y(t_0), z(t_0)] = [-0.1, 0, 0]$. Coexisting attractors under different orders are shown in Figure 7. Obviously, the phase portraits of the CFM system with two symmetric initial values are symmetric, and the system can generate coexisting periodical cycles, chaotic attractors.

In some cases, there is no steady state in the system, and dynamical behaviors of the system are different under certain

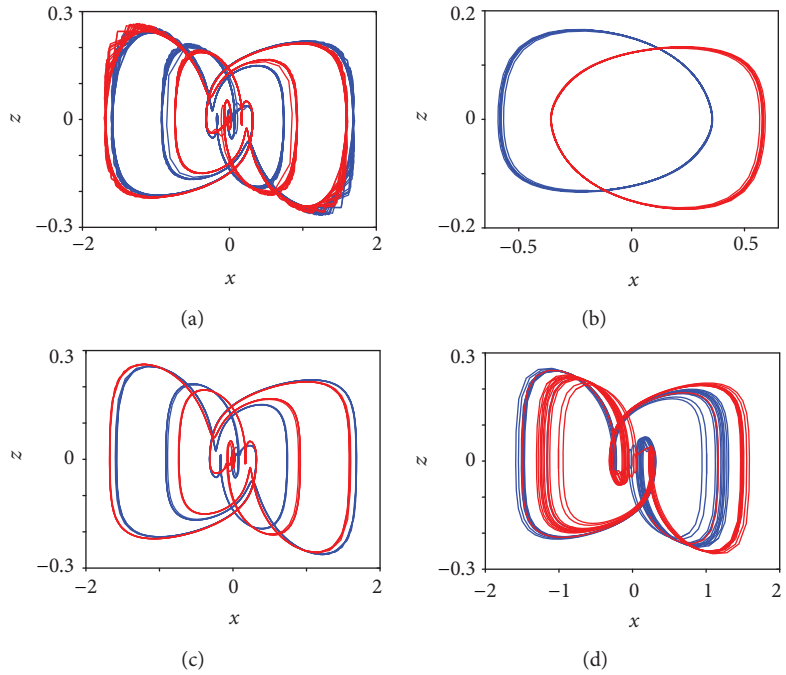

FIGURE 7: Coexisting attractors of the CFM system where $e = 6.9$. The blue line is obtained with the initial condition $[x(t_0), y(t_0), z(t_0)] = [0.1, 0, 0]$, and the red line is obtained with the initial condition $[x(t_0), y(t_0), z(t_0)] = [-0.1, 0, 0]$: (a) $q_1 = q_2 = q_3 = 0.79$; (b) $q_2 = q_3 = 1$, $q_1 = 0.95$; (c) $q_1 = q_3 = 1$, $q_2 = 0.997$; (d) $q_1 = q_2 = 1$, $q_3 = 0.948$.

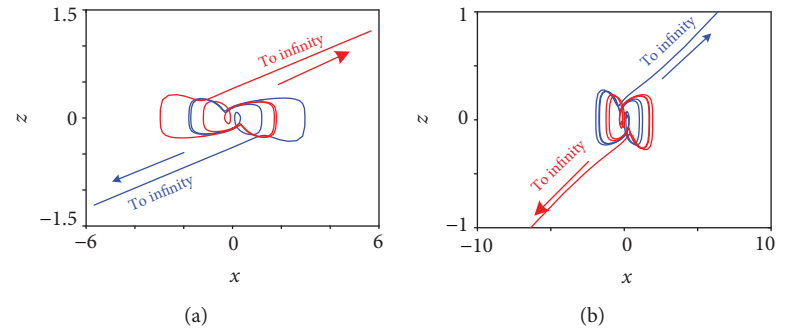

FIGURE 8: Transient state in the CFM system where the blue line is obtained with the initial condition $[x(t_0), y(t_0), z(t_0)] = [0.1, 0, 0]$ and the red line is obtained with the initial condition $[x(t_0), y(t_0), z(t_0)] = [-0.1, 0, 0]$: (a) $q_2 = 0.9955$; (b) $q_2 = 0.9958$.

parameters when starting from a different initial state. As mentioned above, when $e = 6.9$, $q_1 = q_3 = 1$, and $q_2 < 0.9959$, the system has a transient state. Here, phase diagrams with $q_2 = 0.9955$ and 0.9958 are shown in Figure 8, where initial conditions are the same as those mentioned above. The coexisting state and transient state are observed as shown in Figure 8. The system becomes divergent through different directions with different initial conditions, and it is chaotic at the beginning and becomes divergent finally.

4. Complexity Analysis of the CFM System

In this section, complexity of the CFM system is analyzed by means of symbolic complexity measures. Generally, if the system has higher complexity, it means that the system is securer in practical applications. Besides, it is more convenient to calculate complexity since it just needs a segment of time series. Thus, complexity analysis result provides a basis for parameter choice of chaotic systems.

4.1. Symbolic Complexity Measures. In real application, a chaotic time series should be discretized as a pseudorandom sequence or symbolic sequence, which usually varies between 0 and 1 (0-1 time series) or varies from 0 to 255 (8-bit numbers). Here, complexity of chaotic symbolic time series is analyzed using different algorithms including the symbolic entropy (SybEn) algorithm, symbolic spectral entropy (SybSEn) algorithm, and symbolic C_0 (SybC_0) algorithm. These three complexity algorithms are defined as follows.

Step 1 (pseudorandom process). Here, suppose that there is a chaotic series defined as $\{x(n), n = 0, 1, 2, \ldots, N-1\}$; it is

discretized as $\{s(n), n = 0, 1, 2, \dots, N-1\}$ by employing the following method:

$$s(n) = \begin{cases} 0, & \text{if } \min(x) \le x(n) < \Delta x, \\ 1, & \text{if } \Delta x \le x(n) < 2\Delta x, \\ \vdots & \\ 255, & \text{if } 255\Delta x \le x(n) \le \max(x), \end{cases} \tag{14}$$

where $\Delta x = (\max(x) - \min(x))/256$. Thus, $\{s(n), n = 0, 1, 2, \dots, N-1\}$ is an 8-bit number time series.

Step 2 (calculating SybEn). Count the number of each symbol (from 0 to 255), and obtain the probability of each symbol as

$$P_i = \frac{\#\{i : s(n) = i, \quad n = 0, 1, \dots, N-1\}}{N}, \tag{15}$$

where # stands for number and $i = 0, 1, \dots, 255$. Thus, SybEn is defined by

$$\text{SybEn} = -\sum_{i=0}^{255} P_i \log(P_i). \tag{16}$$

Step 3 (discrete Fourier transformation (DFT)). Before the DFT, the following normalization is employed to the symbol time series, and it is denoted as

$$S(n) = \frac{s(n) - \text{mean}(s)}{\text{std}(s)}, \tag{17}$$

where $\text{mean}(s)$ and $\text{std}(s)$ are the mean value and the standard deviation of the time series s, respectively, and $n = 0, 1, \dots, N-1$. Thus, the mean value of the new time is zero and there is no direct current signal. DFT is carried out on time series S, and it is given by

$$X(k) = \sum_{n=0}^{N-1} S(n) e^{-(j2\pi nk/N)}, \tag{18}$$

where $k = 0, 1, \dots, N-1$ and j is the imaginary unit.

Step 4 (calculating SybSEn). If the power of a discrete power spectrum with the kth frequency is $|X(k)|^2$, then the "probability" of this frequency is defined as

$$\rho_k = \frac{|X(k)|^2}{\sum_{k=0}^{N/2-1} |X(k)|^2}. \tag{19}$$

When the DFT is employed, the summation runs from $k = 0$ to $k = N/2 - 1$. The normalization of SybSEn is denoted by [34]

$$\text{SybSEn} = -\frac{1}{\ln(N/2)} \sum_{k=0}^{N/(2-1)} \rho_k \ln \rho_k. \tag{20}$$

$\ln(N/2)$ is the entropy of the completely random signal.

Step 5 (inverse DFT). Define the mean square value of $X(k)$ as

$$G_N = \frac{1}{N} \sum_{k=0}^{N-1} |X(k)|^2. \tag{21}$$

Let

$$\tilde{X}(k) = \begin{cases} X(k), & \text{if } |X(k)|^2 > rG_N, \\ 0, & \text{if } |X(k)|^2 \le rG_N, \end{cases} \tag{22}$$

where $r(r > 0)$ is the control parameter. The inverse DFT of $\tilde{X}(k)$ is

$$\tilde{S}(n) = \frac{1}{N} \sum_{k=0}^{N-1} \tilde{X}(k) e^{j2\pi nk/N}, \tag{23}$$

where $n = 0, 1, \dots, N-1$. $\tilde{S}(n)$ reflects the regular part of the time series with detailed information removed.

Step 6 (calculating SybC_0). SybC_0 complexity is defined as [35]

$$\text{SybC}_0 = \sum_{n=0}^{N-1} \frac{\left|S(n) - \tilde{S}(n)\right|^2}{\Omega}. \tag{24}$$

where $\Omega = \sum_{n=0}^{N-1} |S(n)|^2$.

The three complexity measuring algorithms estimate complexity of an 8-bit symbol time series from different aspects. Firstly, SybEn analyzes complexity in the time domain while SybSEn and SybC_0 are defined in the frequency domain. Secondly, SybEn and SybSEn are defined based on the definition of the Shannon entropy while SybC_0 reflects the ratio of an irregular part in the time series. Let $e = 6.9$ and $q_1 = q_2 = q_3 = 0.95$; we obtain a type II chaotic time series x. The time series is shown in Figure 9(a), and the symbol time series is illustrated in Figure 9(b). By employing (15) and (19), plots of the two different "probabilities" are shown in Figures 9(c) and 9(d), respectively. According to (22) and (24), we illustrate the irregular part of the time series with $r = 10$, where the red line represents $|S(n)|^2$ and the green line represents $\left|S(n) - \tilde{S}(n)\right|^2$ which shows the "difference" or "irregular part."

As shown in Figure 9, the principles of different algorithms are different. For SybEn and SybSEn, if the probability density is more uniform, values of entropy are larger, while if the proportion of the green part is larger, values of SybC_0 are larger. As a result, larger values of SybEn, SybSEn, and SybC_0 mean that the system has higher complexity. In this paper, to analyze the complexity of the CMF system, the time series x with a length of 55000 is sampled with $\tau = 10$; thus, $x = x(1 : 10 : 55000)$. Finally, the sampled time series is changed into a symbol time series. For SybC_0 complexity, we choose $r = 10$.

4.2. Complexity Analysis. Complexity of the CFM system is analyzed by means of SybEn, SybSEn, and SybC_0. Firstly,

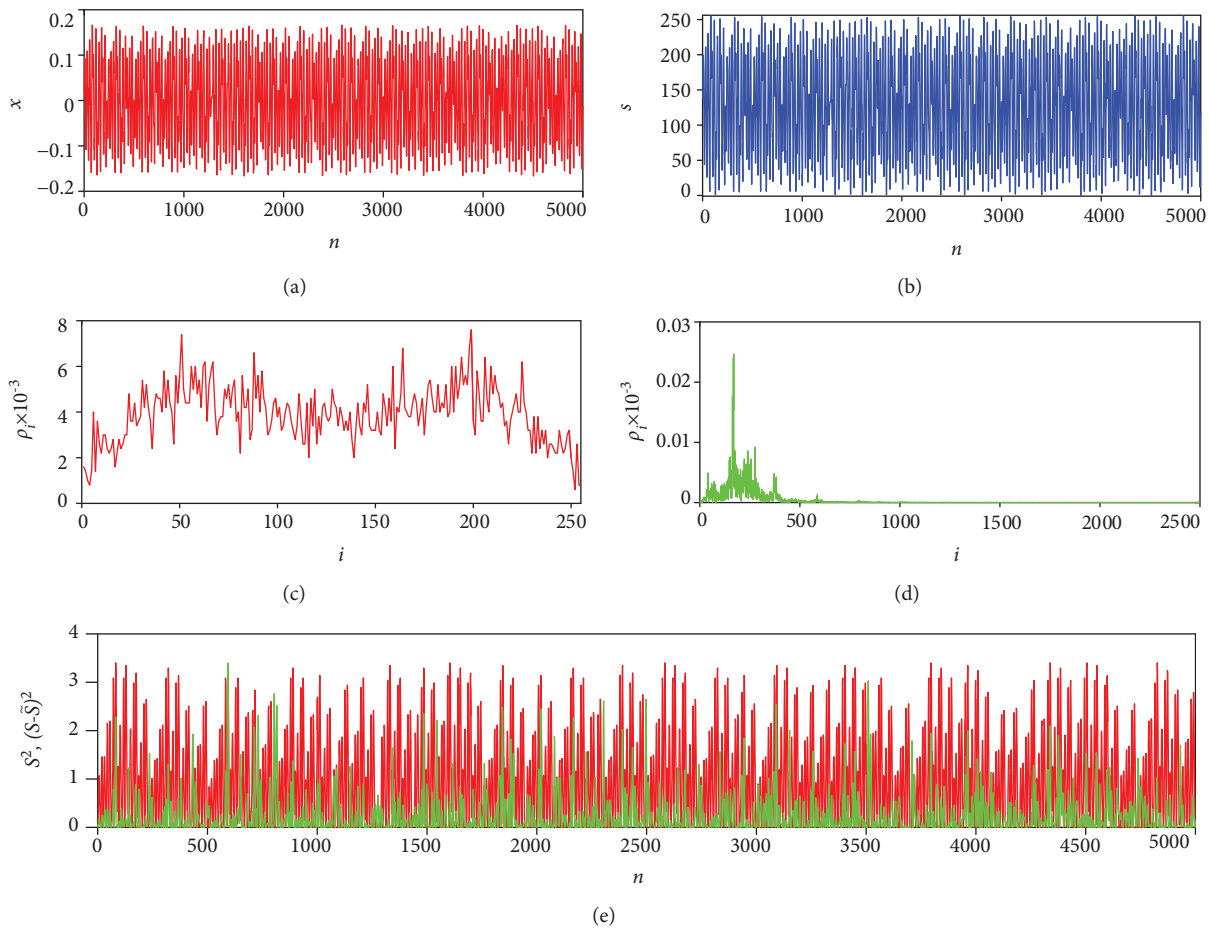

Figure 9: Analysis of complexity algorithms: (a) original time series x; (b) pseudorandom sequence s; (c) probability of each symbol P_i; (d) probability of the frequency ρ_i; (e) irregular part in the SybC$_0$ algorithm.

Table 3: SybEn complexity of the CFM system with different derivative orders.

Type	$q_1 = q_2 = q_3 = 0.95$	$q_1 = q_2 = q_3 = 0.90$	$q_1 = q_2 = q_3 = 0.80$
I	5.4834	5.4646	5.4868
II	4.7810	4.7422	4.6255
III	4.8680	4.8711	4.9467

Table 4: SybSEn complexity of the CFM system with different derivative orders.

Type	$q_1 = q_2 = q_3 = 0.95$	$q_1 = q_2 = q_3 = 0.90$	$q_1 = q_2 = q_3 = 0.80$
I	0.4497	0.5131	0.5589
II	0.5635	0.6135	0.3190
III	0.3580	0.3776	0.5386

SybEn, SybSEn, and SybC$_0$ of different types of CFM systems with different derivative orders are analyzed, and the results are shown in Tables 3–5, respectively. As with Figure 1 and Table 2, values of derivative orders are set as $q_1 = q_2 = q_3 =$ 0.95, 0.90, and 0.80 and $e = 6.9$. It shows that complexity analysis results agree well with the LCE analysis results. When the system is chaotic, higher complexity can be found. Moreover, the system has relative higher complexity when the derivative orders are smaller. It should be pointed out that SybEn cannot distinguish the chaotic state and periodical state well similar to SybSEn and SybC$_0$. Actually, it is also one of the reasons why we furtherly design complexity analysis methods in the frequency domain.

Table 5: SybC$_0$ complexity of the CFM system with different derivative orders.

Type	$q_1 = q_2 = q_3 = 0.95$	$q_1 = q_2 = q_3 = 0.90$	$q_1 = q_2 = q_3 = 0.80$
I	0.1263	0.1756	0.2885
II	0.1913	0.2424	0.0776
III	0.1795	0.1963	0.3128

Complexity of the CFM system with parameter e varying is analyzed, and results are shown in Figure 10. Here, $q_1 = q_2 = q_3 = q$ equals to 0.95, and parameter e varies from 6.7 to 7.05 with a step size of 0.0007. As shown in Figure 10, SybSEn and SybC$_0$ agree with the maximum LCEs better than SybEn, and they identify more periodical windows which show relative lower complexity.

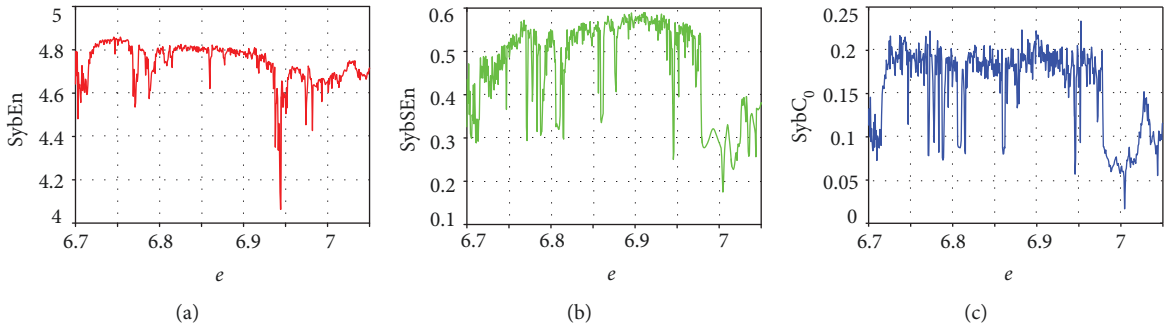

Figure 10: Complexity analysis results of the CFM system with parameter e varying: (a) SybEn; (b) SybSEn; (c) SybC_0.

Complexity of the type II CFM system with parameter $e = 6.9$ and derivative orders q_1, q_2, and q_3 varying is analyzed, and the analysis results are shown in Figure 11. Let $q_1 = q_2 = q_3 = q$ and let it vary from 0.75 to 1. Complexity analysis results are shown in Figures 11(a)–11(c). As shown in Figures 11(b) and 11(c), complexity of the system increases with the decrease of order q, which means that the system has higher complexity with smaller values of q. Thus, the system has a good application value in the engineering field. Fix $q_2 = q_3 = 1$ and vary q_1 from 0.995 to 1, and the complexity results are shown in Figures 11(d)–11(f). Fix $q_1 = q_2 = 1$ and vary q_2 from 0.996 to 1, and the complexity results are displayed in Figures 11(g)–11(i). Moreover, let $q_1 = q_2 = 1$ and vary q_3 from 0.85 to 1, and the complexity results are illustrated in Figures 11(j)–11(l). As shown in those figures, complexity of the CFM system does not increase with the decrease of derivative order q_1, q_2, or q_3. When $q_1 = q_2 = q_3 = 1$, the integer-order system is chaotic with high complexity, but the low-complexity region can be found when the fractional derivative orders decrease. In real application, one should choose those orders with which the system generates high-complexity time series.

According to Figures 11 and 12, SybEn, SybSEn, and SybC_0 complexity analysis results are consistent with the corresponding maximum LCEs to a certain degree. Overall, SybSEn and SybC_0 analysis results agree better with the corresponding maximum LCE results than with those of SybEn. Compared with calculating LCEs, calculating SybEn, SybSEn, and SybC_0 needs much less time and it is more convenient in real application since results can be obtained with a time series. On the one hand, it shows that the system has a potential application value in practice. On the other hand, it provides a basis for parameter choice of the CFM system in real applications.

SybSEn and SybC_0 complexity in the q-e parameter plane is calculated, and the results are shown in Figure 12. Here, the parameter varies from 6.7 to 7.05 similar to that mentioned above, while derivative order q varies from 6.5 to 1, simultaneously. As shown in Figure 12, the minimum order for chaos is about 0.65 when $e = 6.7$. Meanwhile, it shows that the system has higher complexity.

The pseudorandom time series $s(n)$ by (14) fluctuates with the original system variables. As we all know that a chaotic system is a good source for entropy. There are many different kinds of chaotic systems that can be used for designing a pseudorandom sequence generator (PRSG), such as the Lorenz system [39], logistic map, sine map, and 2D-SIMM [40]. And these PRSGs are widely used in real application fields such as image encryption [41], speech encryption [42], and chaotic watermark [43]. The quantization algorithms used in this applications are more complex than the method given in (14). One of the most commonly used methods is designed by expressing the original number or its converted number as a 64-bit binary number as DB_{63}-DB_0; then, one can obtain a new 8-bit number by choosing DB_7-DB_0. The details of this method are given as follows.

The original number is converted as

$$\varphi(n) = \text{round}(x(n) \times 10^{w}), \tag{25}$$

where $n = 0, 1, 2, \ldots, N-1$ and w is a control number. Here, in this paper, $w = 10$. Thus, $\varphi(n)$ is an integer number and it can be expressed as

$$\varphi(n) = \text{DB}_{63}\text{DB}_{62} \cdots \text{DB}_1\text{DB}_0. \tag{26}$$

By choosing the first 8-bit number, a new symbol time series $s(n)$ is given as

$$s(n) = \text{DB}_7 \cdots \text{DB}_1\text{DB}_0. \tag{27}$$

Obviously, $s(n)$ can be expressed as a decimal integer number varying from 0 to 255, as mentioned above. By using this quantization algorithm, complexity of pseudorandom sequences generated by different chaotic systems is calculated and the results are shown in Table 6. The length of each segment symbol time series is 5000, and complexity of such 100 time series is calculated. The results are given as mean ± std of complexity values in these windows. As shown in Table 6, entropy or complexity of different chaotic pseudorandom sequences is at about the same high level. It shows that as with other different chaotic systems, the CFM system is also a good system for high entropy.

According to Table 6, complexity of the CFM system is high as other systems. Thus, it is necessary to check whether the pseudorandom sequence generated by this system passes the test suite of NIST. The package used for the NIST test is sts-2.1.2 which can be downloaded from the website. Two indicators, which are p values and the proportion of passing sequences, are used to show whether the sequence passes the test or not. The minimum value for p value is 0.0001. It

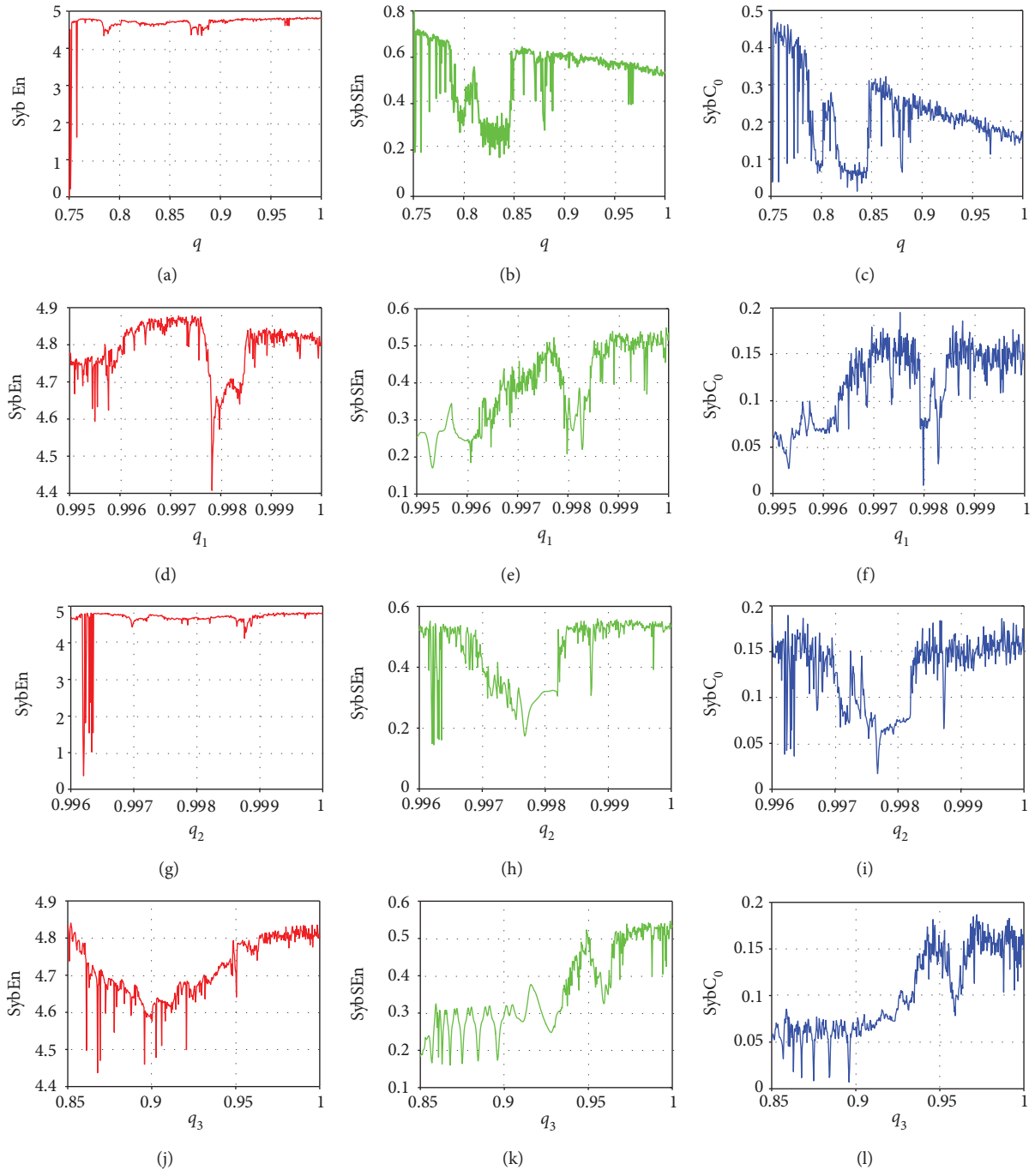

Figure 11: Complexity analysis results of the CFM system with derivative orders varying: (a) SybEn with $q_1 = q_2 = q_3 = q$ varying; (b) SybSEn with $q_1 = q_2 = q_3 = q$ varying; (c) $SybC_0$ with $q_1 = q_2 = q_3 = q$ varying; (d) SybEn with $q_2 = q_3 = 1$ and q_1 varying; (e) SybSEn with $q_2 = q_3 = 1$ and q_1 varying; (f) $SybC_0$ with $q_2 = q_3 = 1$ and q_1 varying; (g) SybEn with $q_1 = q_3 = 1$ and q_2 varying; (h) SybSEn with $q_1 = q_3 = 1$ and q_2 varying; (i) $SybC_0$ with $q_1 = q_3 = 1$ and q_2 varying; (j) SybEn with $q_1 = q_2 = 1$ and q_3 varying; (k) SybSEn with $q_1 = q_2 = 1$ and q_3 varying; (l) $SybC_0$ with $q_1 = q_2 = 1$ and q_3 varying.

means that when the p value is larger than 0.0001 and the confidence interval satisfies

$$\left[(1-\eta) - 3\sqrt{\frac{(1-\eta)\eta}{M}}, (1-\eta) + 3\sqrt{\frac{(1-\eta)\eta}{M}}\right], \tag{28}$$

where M is the sample size and η is the given significance level, then the pseudorandom bit generator passes the test successfully. In our test, the length of the pseudorandom sequence is 10^6, and $\eta = 0.01$ with a confidence interval given by [96.015%, 1]. The test result is illustrated in Table 7. For those items including C. Sums (2 times), N.O. Temp (148

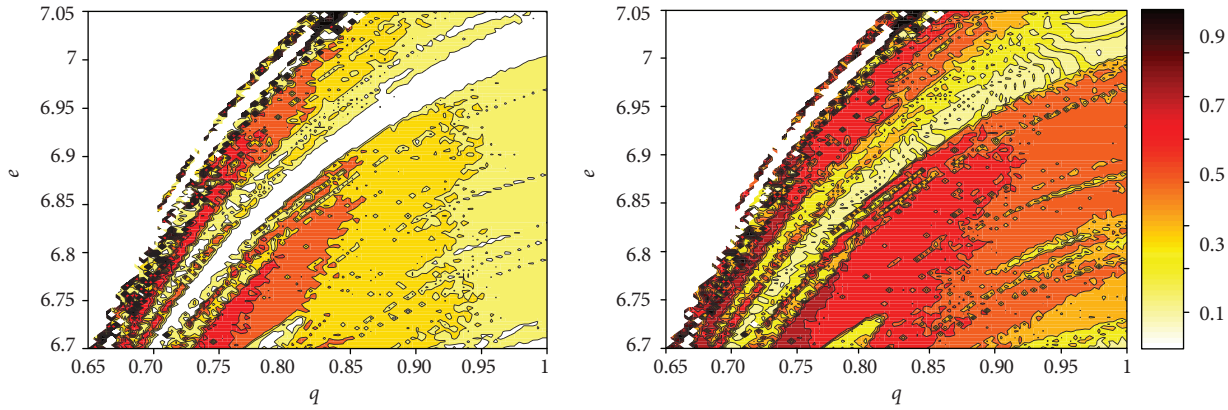

Figure 12: Complexity analysis results of the CFM system in the e-q parameter plane: (a) SybSEn; (b) $SybC_0$.

Table 6: Complexity measuring results of different chaotic pseudorandom sequences with the second quantization method.

Systems	Equations	SybEn	SybSEn	$SybC_0$
CFM system	$T_{t_0}^{q_1} x = cf_1(z)$ $T_{t_0}^{q_2} y = (d-e)f_2(y) + ef_1(z)$ $T_{t_0}^{q_3} z = e(f_2(y) - f_1(z)) - x$	5.4825 ± 0.0036	0.9466 ± 0.0014	0.9995 ± 0.0014
Lorenz system	$\dot{x} = 10(y-x)$ $\dot{y} = 28x - xz - y$ $\dot{z} = (xy - 8z)/3$	5.5206 ± 0.0012	0.9583 ± 0.0003	$0.9995 \pm 4.4 \times 10^{-4}$
Logistic map	$x(n+1) = 4x(n)(1-x(n))$	5.4962 ± 0.0053	0.9461 ± 0.0012	0.9994 ± 0.0015
Sine map	$x(n+1) = 4 \sin(\pi x(n))$	5.4966 ± 0.0043	0.9459 ± 0.0013	0.9992 ± 0.0019
2D-SIMM	$x(n+1) = 10 \sin(\pi y(n)) \sin(10/x(n))$ $y(n+1) = 10 \sin(\pi x(n+1)) \sin(10/y(n))$	5.4966 ± 0.0046	0.9461 ± 0.0014	0.9996 ± 0.0013

times), R. Excur. (8 times), R. Excur. V. (18 times), and Serial (2 times), we only illustrate the lowest values of p value and proportion. It is shown in Table 7 that all p values are larger than 0.0001 and the computed proportion for each test lies inside the confidence interval. Hence, the tested binary sequences generated by the proposed pseudorandom bit generator are random.

In this section, two different pseudorandom quantization algorithms are designed. As shown in Figures 9(a) and 9(b), fluctuation of pseudorandom sequence obtained by the first method given (14) agrees well with the original time series. Thus, it is the reason why complexity analysis results match well with the corresponding maximum LCEs. It provides a good symbol sequence for complexity analysis of chaotic systems when analyzed by complexity measuring methods. However, according to Table 6, pseudorandom sequences generated by different systems by employing the second method have the same level of high complexity. Meanwhile, the pseudorandom sequence passes all the NIST tests. It means that the obtained sequence is random. As with other chaotic systems, the CFM system is also a good secret key generator for real applications including information encryption, secure communication, and chaotic digital watermark.

Table 7: NIST test result of binary sequences generated by the CFM system.

Tests	p value	Proportion	Success
Frequency (1)	0.3345	97/100	✓
B. Frequency (1)	0.6163	100/100	✓
C. Sums (2)	0.9558	99/100	✓
Runs (1)	0.1816	99/100	✓
Longest Run (1)	0.2133	99/100	✓
Rank (1)	0.3191	99/100	✓
FFT (1)	0.1968	99/100	✓
N.O. Temp (148)	0.0288	97/100	✓
O. Temp (1)	0.7197	97/100	✓
Universal (1)	0.5341	99/100	✓
App. Entropy (1)	0.8165	57/58	✓
R. Excur. (8)	0.010	57/58	✓
R. Excur. V. (18)	0.0179	58/58	✓
Serial (2)	0.5544	99/100	✓
L. Complexity (1)	0.1025	99/100	✓

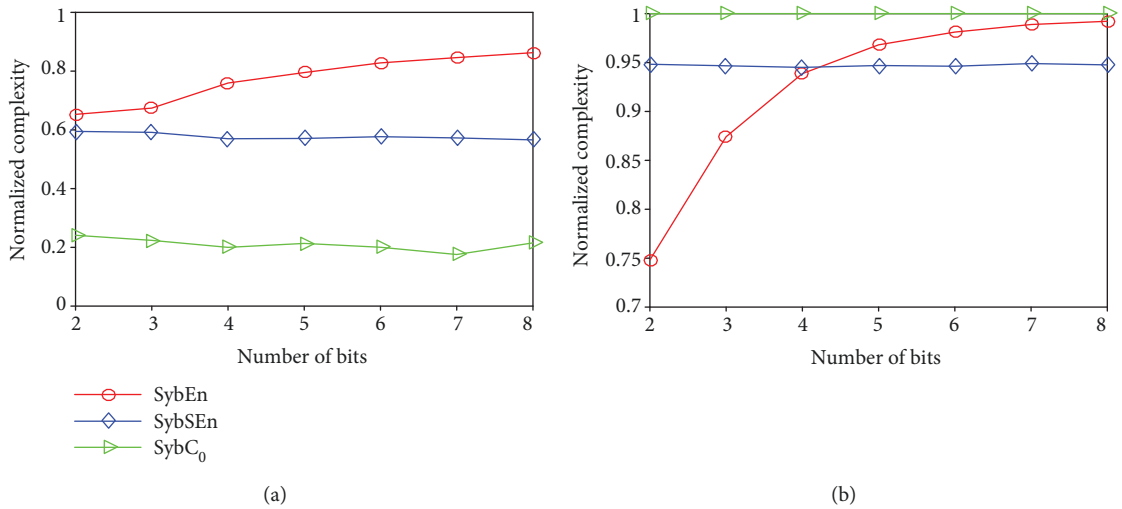

Figure 13: Relation between the number of quantization levels and its complexity: (a) quantization method one; (b) quantization method two.

Finally, it is necessary to explain why we choose 8-bit or 256-quantization-level symbols to form the numbers and how complexity analysis result is determined by the quantization levels. Let $e = 6.9$ and $q_1 = q_2 = q_3 = 0.95$. A segment of type II chaotic time series is used to calculate the complexity. The relation between the number of quantization levels and its complexity measuring results is shown in Figure 13, where SybEn is normalized via dividing $\ln(m)$. Here, m is the number of bits or 2^m is the quantization levels. It shows that the values of the two frequency domain methods, namely, $SybC_0$ and SybSEn, do not change with the quantization levels. However, values of SybEn (the time-domain method) increase but tend to become stable with the quantization levels. Meanwhile, the 8-bit number is widely used in real applications. Thus, 8-bit or 256-quantization-level symbol sequences are employed for complexity analysis.

5. Conclusions

In this work, we introduced the conformable fractional calculus in a nonlinear system with two memcapacitors (CFM system). The conformable fractional differential transform method is employed to solve the nonlinear conformable differential system for the first time. The ALCE calculation algorithm is designed based on the obtained solution, and bifurcation and chaos in the CFM system are explored. It shows that the CFM system has rich dynamics with the variation of system parameter and derivative orders. Meanwhile, coexisting attractors and transient state were observed under some specific parameters. Three symbol complexity measuring algorithms are designed, namely, symbolic entropy (SybEn) algorithm, symbolic spectral entropy (SybSEn) algorithm, and symbolic C_0 ($SybC_0$) algorithm. Complexity analysis results match well with the corresponding maximum LCE analysis results. Finally, by using a proper quantization algorithm, the obtained pseudorandom sequence has high complexity as other common chaotic systems and is randomly verified by the NIST test. It shows that the memory electronic element-based systems have a potential engineering application value.

Data Availability

The data used to support the findings of this study are included within the article.

Conflicts of Interest

The authors declare that there is no conflict of interest regarding the publication of this paper.

Acknowledgments

Shaobo He acknowledges the support from the Post-Doctoral Innovation Talent Support Program (no. BX20180386), the National Natural Science Foundation of China (no. 11747150), the Natural Science Foundation of Hunan Province (no. 2018JJ4015), and the Foundation of Hunan University of Arts and Science (nos. E07016048 and 17BSQD07).

References

[1] L. O. Chua, "Memristor-the missing circuit element," *IEEE Transactions on Circuit Theory*, vol. 18, no. 5, pp. 507–519, 1971.

[2] D. B. Strukov, G. S. Snider, D. R. Stewart, and R. S. Williams, "The missing memristor found," *Nature*, vol. 453, no. 7191, pp. 80–83, 2008.

[3] H. Kim, M. P. Sah, C. Yang, T. Roska, and L. O. Chua, "Neural synaptic weighting with a pulse-based memristor circuit," *IEEE Transactions on Circuits and Systems I: Regular Papers*, vol. 59, no. 1, pp. 148–158, 2012.

[4] Y. Babacan, F. Kaçar, and K. Gürkan, "A spiking and bursting neuron circuit based on memristor," *Neurocomputing*, vol. 203, pp. 86–91, 2016.

[5] C. Sánchez-López, J. Mendoza-López, M. A. Carrasco-Aguilar, and C. Muñiz-Montero, "A floating analog memristor emulator circuit," *IEEE Transactions on Circuits and Systems II: Express Briefs*, vol. 61, no. 5, pp. 309–313, 2017.

[6] M. D. Ventra, Y. V. Pershin, and L. O. Chua, "Circuit elements with memory: memristors, memcapacitors, and meminductors," *Proceedings of the IEEE*, vol. 97, no. 10, pp. 1717–1724, 2009.

[7] D. Biolek and V. Biolkova, "Mutator for transforming memristor into memcapacitor," *Electronics Letters*, vol. 46, no. 21, pp. 1428-1429, 2010.

[8] B. C. Bao, Q. Xu, H. Bao, and Q. Xu, "Extreme multistability in a memristive circuit," *Electronics Letters*, vol. 52, no. 12, pp. 1008–1010, 2016.

[9] B. C. Bao, P. Y. Wu, H. Bao, M. Chen, and Q. Xu, "Chaotic bursting in memristive diode bridge-coupled Sallen-Key lowpass filter," *Electronics Letters*, vol. 53, no. 16, pp. 1104-1105, 2017.

[10] B. C. Bao, L. Xu, Z. M. Wu, M. Chen, and H. Wu, "Coexistence of multiple bifurcation modes in memristive diode-bridge-based canonical Chua's circuit," *International Journal of Electronics*, vol. 105, no. 7, pp. 1159–1169, 2018.

[11] B. C. Bao, P. Y. Wu, H. Bao, Q. Xu, and M. Chen, "Numerical and experimental confirmations of quasi-periodic behavior and chaotic bursting in third-order autonomous memristive oscillator," *Chaos, Solitons & Fractals*, vol. 106, pp. 161–170, 2018.

[12] J. Mou, K. Sun, J. Ruan, and S. He, "A nonlinear circuit with two memcapacitors," *Nonlinear Dynamics*, vol. 86, no. 3, pp. 1735–1744, 2016.

[13] L. Zou, Y. Peng, Y. Feng, and Z. Tu, "Stabilization and synchronization of memristive chaotic circuits by impulsive control," *Complexity*, vol. 2017, Article ID 5186714, 10 pages, 2017.

[14] J. Kengne, A. N. Negou, and D. Tchiotsop, "Antimonotonicity, chaos and multiple attractors in a novel autonomous memristor-based jerk circuit," *Nonlinear Dynamics*, vol. 88, no. 4, pp. 2589–2608, 2017.

[15] S. Kumar, J. P. Strachan, and R. S. Williams, "Chaotic dynamics in nanoscale NbO_2 Mott memristors for analogue computing," *Nature*, vol. 548, no. 7667, pp. 318–321, 2017.

[16] B. Wang, F. C. Zou, and J. Cheng, "A memristor-based chaotic system and its application in image encryption," *Optik - International Journal for Light and Electron Optics*, vol. 154, pp. 538–544, 2018.

[17] S. B. He, K. H. Sun, and H. H. Wang, "Complexity analysis and DSP implementation of the fractional-order Lorenz hyperchaotic system," *Entropy*, vol. 17, no. 12, pp. 8299–8311, 2015.

[18] S. B. He, K. H. Sun, and H. H. Wang, "Solution and dynamics analysis of a fractional-order hyperchaotic system," *Mathematical Methods in the Applied Sciences*, vol. 39, no. 11, pp. 2965–2973, 2016.

[19] K. Rajagopal, A. Karthikeyan, and A. K. Srinivasan, "FPGA implementation of novel fractional-order chaotic systems with two equilibriums and no equilibrium and its adaptive sliding mode synchronization," *Nonlinear Dynamics*, vol. 87, no. 4, pp. 2281–2304, 2017.

[20] R. Zhang and S. Yang, "Robust synchronization of two different fractional-order chaotic systems with unknown parameters using adaptive sliding mode approach," *Nonlinear Dynamics*, vol. 71, no. 1-2, pp. 269–278, 2013.

[21] K. Rajagopal, L. Guessas, A. Karthikeyan, A. Srinivasan, and G. Adam, "Fractional order memristor no equilibrium chaotic system with its adaptive sliding mode synchronization and genetically optimized fractional order PID synchronization," *Complexity*, vol. 2017, no. 4, 19 pages, 2017.

[22] D. Cafagna and G. Grassi, "On the simplest fractional-order memristor-based chaotic system," *Nonlinear Dynamics*, vol. 70, no. 2, pp. 1185–1197, 2012.

[23] R. Gorenflo and F. Mainardi, "Fractional calculus: integral and differential equations of fractional order," *Mathematics*, vol. 49, no. 2, pp. 277–290, 2012.

[24] R. Khalil, M. A. Horani, A. Yousef, and M. Sababheh, "A new definition of fractional derivative," *Journal of Computational and Applied Mathematics*, vol. 264, no. 5, pp. 65–70, 2014.

[25] T. Abdeljawad, "On conformable fractional calculus," *Journal of Computational and Applied Mathematics*, vol. 279, pp. 57–66, 2014.

[26] B. B. İskender Eroğlu, D. Avcı, and N. Özdemir, "Optimal control problem for a conformable fractional heat conduction equation," *Acta Physica Polonica A*, vol. 132, no. 3, pp. 658–662, 2017.

[27] M. S. Hashemi, "Invariant subspaces admitted by fractional differential equations with conformable derivatives," *Chaos, Solitons & Fractals*, vol. 107, pp. 161–169, 2018.

[28] N. A. Khan, O. A. Razzaq, and M. Ayaz, "Some properties and applications of conformable fractional Laplace transform (CFLT)," *Journal of Fractional Calculus and Applications*, vol. 9, no. 1, pp. 72–81, 2018.

[29] S. B. He, K. H. Sun, X. Y. Mei, B. Yan, and S. Xu, "Numerical analysis of a fractional-order chaotic system based on conformable fractional-order derivative," *The European Physical Journal Plus*, vol. 132, no. 1, pp. 1–11, 2017.

[30] J. Ruan, K. Sun, J. Mou, S. He, and L. Zhang, "Fractional-order simplest memristor-based chaotic circuit with new derivative," *The European Physical Journal Plus*, vol. 133, no. 1, pp. 1–10, 2018.

[31] E. Ünal and A. Gökdoğan, "Solution of conformable fractional ordinary differential equations via differential transform method," *Optik - International Journal for Light and Electron Optics*, vol. 128, pp. 264–273, 2017.

[32] S. A. Makarkin, A. V. Starodubov, and Y. A. Kalinin, "Application of permutation entropy method in the analysis of chaotic, noisy, and chaotic noisy series," *Technical Physics*, vol. 62, no. 11, pp. 1714–1719, 2017.

[33] S. N. Yu and M. Y. Lee, "Wavelet-based multiscale sample entropy and chaotic features for congestive heart failure recognition using heart rate variability," *Journal of Medical and Biological Engineering*, vol. 35, no. 3, pp. 338–347, 2015.

[34] C. C. Hwang, "On the normalized spectral entropy of the chaotic states," *Journal of Non-Equilibrium Thermodynamics*, vol. 21, no. 3, pp. 270–277, 1996.

[35] Z. J. Cai and J. Sun, "Convergence of C_0 complexity," *International Journal of Bifurcation and Chaos*, vol. 19, no. 3, pp. 977–992, 2009.

[36] W. Yao and J. Wang, "Double symbolic joint entropy in nonlinear dynamic complexity analysis," *AIP Advances*, vol. 7, no. 7, pp. 1031–1051, 2017.

[37] Y. Li, Y. Yang, G. Li, M. Xu, and W. Huang, "A fault diagnosis scheme for planetary gearboxes using modified multi-scale symbolic dynamic entropy and mRMR feature selection," *Mechanical Systems and Signal Processing*, vol. 91, pp. 295–312, 2017.

[38] H. F. V. Bremen, F. E. Udwadia, and W. Proskurowski, "An efficient QR based method for the computation of Lyapunov exponents," *Physica D: Nonlinear Phenomena*, vol. 101, no. 1-2, pp. 1–16, 1997.

[39] C. Sparrow, "The Lorenz equations: bifurcations, chaos, and strange attractors," in *Applied Mathematical Sciences*Springer, New York.

[40] W. H. Liu, K. H. Sun, and C. X. Zhu, "A fast image encryption algorithm based on chaotic map," *Optics and Lasers in Engineering*, vol. 84, pp. 26–36, 2016.

[41] R. Parvaz and M. Zarebnia, "A combination chaotic system and application in color image encryption," *Optics & Laser Technology*, vol. 101, pp. 30–41, 2018.

[42] J. S. Long, "A speech encryption using fractional chaotic systems," *Nonlinear Dynamics*, vol. 65, no. 1-2, pp. 103–108, 2010.

[43] P. Raj and M. Gurjar, "Discrete wavelet transform and chaotic map based watermark hiding in medical images," *International Journal of Computer Applications*, vol. 177, no. 1, pp. 21–26, 2017.